

Research Article

Ionospheric Response to November 5-6, 2023 Geomagnetic Storm over West African Sector

Gebre Kalute^{1,*} , Dejene Ambisa^{1,2} , Selemon Sisay¹ , Tegegn Teferi¹ 

¹Department of Physics, Wolaita Sodo University, Wolaita Sodo, Ethiopia

²Department of Space and Planetary Science, Space Science and Geospatial Institute, Addis Ababa, Ethiopia

Abstract

This paper investigates the response of the ionosphere to November 5-6, 2023 geomagnetic storm in West African sectors. The November 5-6, 2023 geomagnetic storm, a significant space weather event, had profound effects on the ionosphere over the West African sector, particularly in countries such as Ghana, Senegal, Benin, Cabo Verde, and Cote d'Ivoire. To investigate the ionospheric response during this storm, the study focused on key parameters such as Total Electron Content (TEC), solar wind conditions, and the horizontal component of Earth's magnetic field. Using data from GNSS/GPS stations, thermospheric neutral composition measurements, and satellite observations, the analysis reveals marked variations in TEC and other ionospheric parameters, indicating a strong ionospheric response. The analysis of TEC revealed marked variations during the storm, with significant positive ionospheric storm phases observed in countries such as ACRG; Ghana and YKR; Cote d'Ivoire, with TEC values on both November 5 and 6 are significantly higher than the quiet day mean, especially during the early afternoon hours (10:00 UT to 18:00 UT). In contrast, the TEC variations in DAKR; Senegal, CPVG; Cabo Verde and BJC; Benin were less pronounced, suggesting a weaker storm influence in these regions. The relative proximity of these stations to the geomagnetic equator might account for the observed differences, as the equatorial ionosphere is known to respond differently to geomagnetic disturbances compared to higher latitudes. The results highlight the complex interactions between solar wind, geomagnetic activity, and ionospheric conditions in the West African region, providing valuable insights for understanding and predicting ionospheric disturbances. The storm also had a noticeable effect on the thermospheric composition, as indicated by changes in the O/N₂ ratio. The result suggests that the thermosphere experienced a slight relaxation in storm effects by November 6, but with some residual disturbances. Additionally, the prompt penetration electric field model, (PPEFM) effectively captured the behavior of the prompt penetration electric field, PPEF, which intensified or suppressed the prereversal enhancement (PRE) during the postsunset period in the main phase of the March 5-6, 2023, storms.

Keywords

Ionosphere, Geomagnetic Storm, West Africa, Total Electron Content (TEC), Thermospheric Composition

1. Introduction

The top layer of the atmosphere, known as the ionosphere, is created when atoms and molecules in that area become

ionized due to solar radiation [1]. Since a few decades ago, ionosphere experts have been closely monitoring alterations

*Corresponding author: gebrekaluteg@gmail.com (Gebre Kalute)

Received: 16 January 2025; **Accepted:** 22 April 2025; **Published:** 26 May 2025



Copyright: © The Author(s), 2025. Published by Science Publishing Group. This is an **Open Access** article, distributed under the terms of the Creative Commons Attribution 4.0 License (<http://creativecommons.org/licenses/by/4.0/>), which permits unrestricted use, distribution and reproduction in any medium, provided the original work is properly cited.

in the ionosphere caused by geomagnetic storms. An extreme type of space weather known as ionospheric storms has a major negative impact on our society's increasingly complex ground- and space-based technological systems [2]. The ionosphere has been divided into regions (D, E, and F), with the term "layer" referring to the ionization within a region. The lowest is the D-region, covering altitudes between about 50 and 90 km. The E-region lies between 90 and 150 km, and the F-region is the ionosphere above the E-region and it is the layer where electron concentrations reach their highest value. The F-zone is the most crucial area in the ionosphere for long-distance HF radio communications [3]. In the upper regions of the ionosphere, beginning several hundred kilometres above Earth's surface and extending tens of thousands of kilometres into space, is the magnetosphere, a region where the behavior of charged particles is strongly affected by the magnetic fields of Earth and the Sun [4]. The ionosphere varies greatly because of changes in sources of ionization and response to changes in the neutral part of the upper atmosphere in which it is embedded. This region of the atmosphere is known as the thermosphere. Since it responds to solar EUV radiation, the ionosphere varies over the 24-hour period between day-time and night-time [5]. The Ionospheric regular variations exhibit distinctive patterns across different temporal scales. Diurnal variations, for instance, manifest as daily oscillations in electron density, with peaks typically occurring around local noon and nighttime minima [6].

The physical and chemical behavior of ionosphere is affected by a variety of natural and man-made processes [7]. Among these factors, solar eclipses and geomagnetic storms, both of which directly affect the Earth's ionosphere [8]. A significant disruption of the geomagnetic field brought on by solar activity is known as a geomagnetic storm (GMS) [9]. The main causes for the geomagnetic storms on Earth are powerful interplanetary electric fields brought on by magnetic fields oriented southward passing past the planet for an extended enough period of time Gonzalez et al. (1994) and it is also caused variation in the solar wind parameters, that is enhancement in solar wind speed and solar wind particles that increase solar wind pressure [10, 11]. When the B_z component of the magnetic fields are substantially negative, open field lines are created by magnetic reconnection between the geomagnetic field and the interplanetary magnetic field (IMF B_z). This allows mass, energy, and momentum to be transported from the solar wind to the Earth's magnetosphere [12]. During a magnetic storm, the thermospheric circulation and changes in neutral composition can both affect the ionospheric variation [13]. The ionospheric disturbances are caused by sudden changes in magnetospheric fields, currents, and plasmas, which are carried to the Earth's atmosphere through coupling mechanisms in the form of particle precipitation, joule heating, and energy dissipation. The ionosphere gets significant disturbances during geomagnetic storms, performing in changes in electron viscosity and ionospheric parameters [14].

Geomagnetic storms can have a significant impact on the Earth's ionosphere. During geomagnetic storms, the increased solar activity and disturbances in the Earth's magnetic field can lead to changes in the ionosphere's density, temperature, and composition [15]. It can cause disturbances in the ionosphere, leading to irregularities in electron density distribution. This can impact the dynamics of the ionosphere and lead to disruptions in radio communication systems. Geomagnetic storms can also induce plasma instabilities in the ionosphere, leading to the formation of plasma bubbles and irregularities [16]. Because disturbances of TEC, electron peak density, and electron peak height are produced, the study of the ionospheric disturbances during geomagnetic storms is typically conducted using either the critical frequency of the F2 layer (f_{F2}) or TEC. In line with peak electron density, during storm phases, TEC may rise or fall in relation to levels under tranquil conditions. The ionospheric features of the electron density during the various phases of the geomagnetic storms at different latitudes have been explained by a variety of dynamical and chemical processes, including energetic particle precipitation, changes in electric field and current systems, traveling atmospheric disturbances, thermospheric circulation, composition changes, etc. Ionospheric storms are complicated by these characteristics [17].

Investigating the ionospheric dynamics and disturbances during geomagnetic storms has become crucial and remains one of the key questions in space physics [18]. On this regards, numerous researches have examined how the ionosphere at low latitudes reacts to magnetic storm occurrences [19]. Among those, the studies conducted by Olawepo, (2013) on low latitudinal ionosphere responses during magnetic storm periods have been an inspiration for us to choose this research area [20]. Olawepo, & Adeniyi, (2012) used two GNSS stations over Nigeria have been used to examine the effects of the St. Patrick's Day geomagnetic storms in 2013 and 2015 [21]. The researchers observed variations in TEC, which correlated with changes in positioning inaccuracy resulting from the latitudinal variance between the two study sites [22]. Despite being researched for several decades, the ionospheric disturbances caused by geomagnetic storms, also known as ionospheric storms, continue to be one of the pillars of near-Earth space physics (e.g., Astafyeva et al., (2015); Zolotukhina et al., (2017)) [23, 24]. This is due to the fact that ionospheric disturbances lead to major interruptions in satellite positioning and radio wave communications, among other things, and that there are various variations in the behavior of ionospheric parameters during storms.

The studies described above mainly focused on observations of the response of the ionosphere due to the storm at different latitudes and longitudes in others parts of West Africa. However, in this regard, the investigation of ionospheric response to a geomagnetic storm that occurred in November 2023 5-6, over Ghana, Senegal, Benin, Cabo Verde and, Cote d'Ivoire is not yet studied in detail. Thus this work determines the variations in ionospheric parameters such total electron

content, and solar wind parameters during the storm event in November 2023 5-6, over Ghana, Senegal, Benin, Cabo Verde and, Cote d'Ivoire. Investigating the ionospheric response to a geomagnetic storm provides valuable insights into the complex interactions between the Earth's magnetic field and the solar wind. The rest of the paper is organized as follows: Section 2 describes the data sets and techniques of data analysis, Section 3 presents analysis of the results, Section 4 is discussions based on the result and then the final Section 5 come up with conclusion.

2. Data Sets and Method

2.1. Solar Wind Parameters and Geomagnetic Indices

To analyze the ionospheric response over West African sector, we considered different solar wind parameters and a geomagnetic indice. Particularly, in this paper, the solar wind parameters such as, solar wind speed (V_{sw}), solar wind dynamical pressure (P_{sw}) and interplanetary magnetic field data, IMF (B_z) were obtained from (ACE Science Center, (<http://www.srl.caltech.edu/ACE/>) and OMNIWeb interface at (<https://omniweb.gsfc.nasa.gov/>) and geomagnetic activity index like SYM-H used to describe the geomagnetic storm condition during November 5-6, 2023 is obtained from Kyoto World Data Center (<http://wdc.kugi.kyoto-u.ac.jp/wdc/Sec3.html>). SYM-H has a 1-minute resolution, providing finer temporal details compared to indices like Dst index, which is recorded hourly. This high resolution allows us to capture rapid changes in geo-

magnetic activity, especially during the initial and main phases of geomagnetic storms, which are crucial for studying ionospheric responses.

2.2. GNSS-GPS TEC Data

GNSS/GPS is the most commonly used for research purposes, including studying the ionospheric response to geomagnetic storms. GPS has a wide coverage and availability of stations in the region, making it a popular choice for ionosphere-related studies [25]. TEC plays a vital role in ionospheric research as it provides a measure of the total number of electrons present along the path of a GPS signal as it travels from a satellite to a ground-based receiver. These TEC values are particularly important in understanding how the ionosphere behaves during geomagnetic storms, which can lead to notable variations in electron density. During geomagnetic storms, the increased energy from the Sun interacts with Earth's magnetic field, causing disturbances that lead to changes in ionospheric electron content. These changes can be observed as significant fluctuations in TEC values. By analyzing these variations, researchers can gain valuable insights into the impact of geomagnetic activity on the ionosphere. GNSS/GPS receivers' data in receiver-independent exchange (RINEX) format available at: NASA Crustal Dynamics Data Information System (CDDIS) archive (<ftp://cddis.gsfc.nasa.gov/pub/gps/data/daily/>), AFREF (<http://www.afrefdata.org/>) and IGS (<http://igs.org>), were used to derive TEC values [26]. The geographic and geomagnetic coordinates of the station used were listed below in Table 1 along its map.

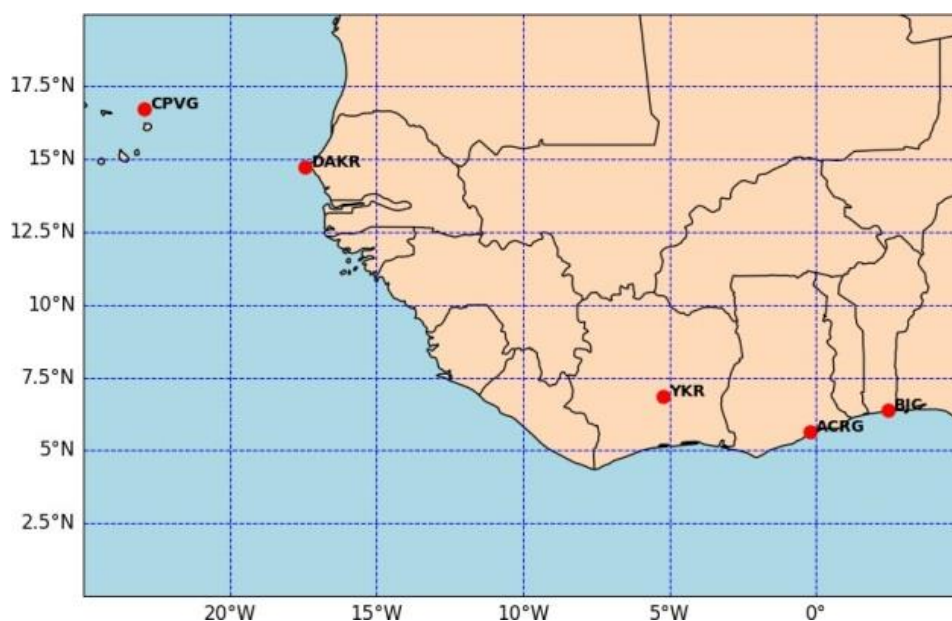


Figure 1. Map with the stations used in this study.

Table 1. Geographical locations of the stations used in the study.

IGS Stations	Geog. Lat.	Geog. Long.	Geomag. Lat.	Geomag. Long.
ACRG, Ghana	5.641	-0.207	-7.06	74.23
BJC, Benin	6.385	2.45	-6.12	77.03
CPVG, Cabo Verde	16.735	-22.935	6.22	52.35
DAKR, Senegal	14.721	-17.439	3.25	57.35
YKR, Cote d'Ivoire	6.871	-5.24	-5.87	69.03

2.3. Thermospheric Neutral Composition

The thermospheric neutral composition, specifically the global O/N₂ ratio, was served as another vital parameter in this study. This O/N₂ ratio is known to undergo significant variations during geomagnetic storms and is a critical factor influencing the ionospheric response. Thus to analyze storm-time variations in the thermospheric neutral composition, global O/N₂ ratios measured by the Global Ultraviolet Imager (GUVI) on NASA's Thermosphere Ionosphere Mesosphere Energetics and Dynamics (TIMED) satellite (<http://guvitimed.jhuapl.edu>) were utilized [27]. This data was employed to assess the changes in thermospheric composition that occurred during the geomagnetic storm periods.

2.4. Prompt Penetration Equatorial Electric Field Model Data (PPEFM)

To better understand the variation of Prompt penetration equatorial electric field (PPEF) during the main phase of storms, the PPEFM was employed to estimate the PPEF in the African sector [28]. The PPEFM data used in this study was obtained from the NOAA Space Weather Prediction Center in collaboration with CIRES at the University of Colorado Boulder, available at <https://geomag.colorado.edu/online-calculators/real-time-model-ionospheric-electric-fields>. This model functions as a transfer mechanism that simulates daily changes in equatorial ionospheric electric fields using solar wind IEF data. Further details are provided in [29]. The model's inputs include time and location, while the outputs are estimated values of the equatorial electric field (EEF), specifically: (i) the background electric field (representing the quiet electric field observed during geomagnetically calm conditions) and (ii) the total electric field (which is the sum of the quiet electric field and the prompt penetration electric field).

2.5. Data Processing

The data were analyzed using specialized software, with MATLAB utilized for time-series analysis and visualization.

Total Electron Content (TEC) values were extracted from RINEX files using a tool developed by Dr. Gopi Krishna Seemala from the Indian Institute of Geomagnetism. This tool, available at <https://seemala.blogspot.com/>, is calibrated to correct for signal delays caused by ionospheric electron density. It provides high-precision TEC measurements, which are essential for monitoring ionospheric variations during geomagnetic storms. During November 2023, five international quiet days were selected to compute the average of them as a single day. Also 05 and 06 November 2023 were considered as the international storm days during November 2023. The average TEC values seen on quiet days were plotted here to acted as a reference point for comparison during storm weather diurnal TEC variation of 05 and 06 November 2023 over West Africa, of those five selected stations.

Solar wind parameters, including IMF B_z, and wind speed, are resampled to match SYM-H's 1-minute resolution, with derived quantities like dynamic pressure extracted for correlation analysis with geomagnetic indices. O/N₂ data from satellites such as TIMED/GUVI is interpolated, converted to magnetic coordinates, and analyzed to map storm-time variations, with changes compared to total electron content (TEC) and equatorial anomalies. PPEF data, modeled using inputs like IMF B_z and solar wind velocity or derived from satellite observations, is validated and assessed for its role in driving equatorial ionospheric currents and TEC variations, particularly during storm phases. Temporal synchronization of all datasets allows for cross-correlation and time-lagged analyses, focusing on specific storm events to link solar wind dynamics, geomagnetic indices, and ionospheric parameters.

3. Results

3.1. Geophysical Condition During November 3-8, 2023

November 3 was characterized by quiet space weather conditions, with no significant geomagnetic activity or disturbances in the Earth's magnetosphere, with solar wind speed is relatively low around 350 km/s, dynamic pressure below 5nPa, with no significant southward or northward B_z compo-

ment, and stable Sym-H index around zero. Like November 3, November 4 was also a quiet day in terms of space weather, with stable geomagnetic conditions and no significant disturbances. The solar wind speed remains similar to November 3, around 350-400 km/s. There is a slight increase in dynamic pressure to around 5-10 nPa, but still within a quiet range. The Bz component shows some minor fluctuations but does not reach significant southward values and the Sym-H index remains stable near zero, indicating continued quiet geomagnetic conditions.

The solar wind speed (V_{SW}) (green line) was relatively stable around 300-400 km/s before the storm. On November 5, around 12:00 UT, there was a sudden increase in the solar wind speed, reaching over 600 km/s, indicating the arrival of a high-speed solar wind stream or a coronal mass ejection (CME). This increase in speed is one of the triggers for geomagnetic storms as it enhances the interaction between the

solar wind and the Earth's magnetosphere. The solar wind dynamic pressure (blue color) remained low and stable before the storm but showed a significant increase around the same time as the solar wind speed, reaching nearly 20 nPa.

Elevated solar wind pressure can compress the magnetosphere, leading to increased geomagnetic activity. The Bz (red line) component fluctuates around zero before the storm but turns sharply southward (negative) just before the onset of the main phase of the storm. A southward Bz is critical for storm development because it allows magnetic reconnection with the Earth's magnetic field, facilitating energy transfer from the solar wind into the magnetosphere. Bz remained negative during the main phase of the storm, which would have sustained geomagnetic activity, and then it turned northward (positive) during the recovery phase, which typically signifies the end of the storm's impact.

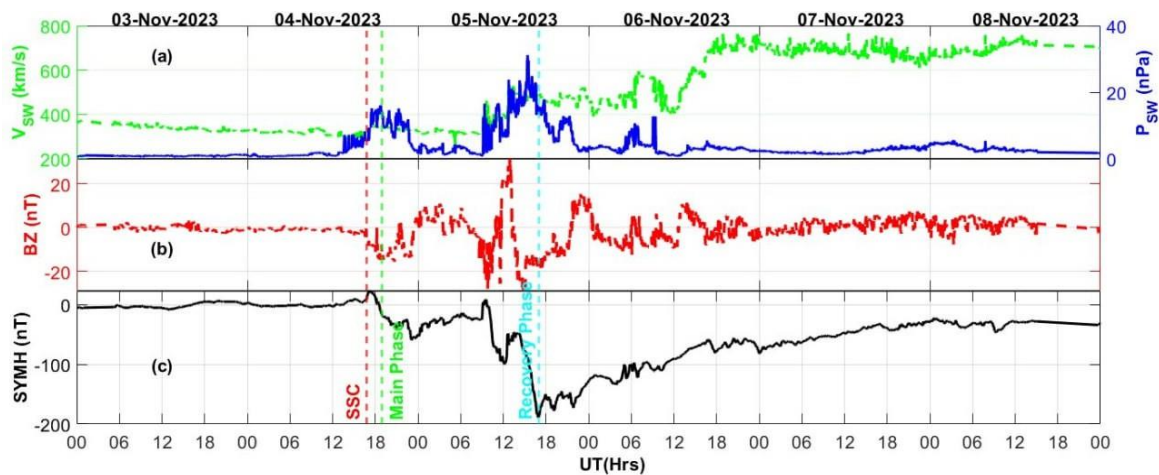


Figure 2. Geomagnetic indices and solar wind parameters before, during and after the storm period (03-08, November 2023).

The Sym-H index (black color) is a proxy for the disturbance in the Earth's magnetosphere and can be used to monitor geomagnetic storms. On November 5, the Sym-H index shows a sharp drop starting around 18:00 UT, marking the onset of the main phase of the storm. The index reached a minimum of around -100 nT, indicating a strong geomagnetic storm. The recovery phase begins soon after, as seen by the gradual return of the Sym-H index towards zero over the next 24 hours. Storm Sudden Commencement (SSC), marked by the vertical red dashed line around 17:00 UT on November 5, 2023, corresponds to the sudden increase in solar wind speed and pressure. This is the point where the storm began. The main phase, indicated by the green dashed line, follows shortly after the SSC, where the Bz component turns strongly southward and the Sym-H index drops sharply. This phase represents the peak of the geomagnetic storm, characterized by intense geomagnetic activity and disturbances in the ionosphere. After the storm, the solar wind speed decreases from the elevated levels seen during the storm, returning to around

450-500 km/s.

The dynamic pressure remains slightly elevated, around 10-15 nPa, but not as high as during the storm. The Bz component shows some fluctuations but generally remains near zero or slightly northward. The recovery phase, marked by the blue dashed line on November 6, occurs as the Bz component returns northward, and the Sym-H index starts to recover. During this phase, the magnetosphere begins to return to its normal state, and the geomagnetic activity diminishes. Thus, November 7 marks the recovery phase after the geomagnetic storm. Geophysical conditions are stabilizing, but the effects of the storm are still lingering, as seen in the slightly elevated solar wind parameters and the Sym-H index's slow recovery. On November 8, 2023, the solar wind speed continues to decrease, stabilizing around 400 km/s. The dynamic pressure remains steady around 10 nPa. The Bz component is relatively stable and fluctuates around zero, showing no significant southward excursions. The Sym-H index has mostly returned to near zero, indicating that the geomagnetic storm has fully

subsided and geomagnetic conditions are now quiet. In general, By November 8, the geomagnetic conditions have largely returned to quiet levels. The magnetosphere has recovered from the storm, and space weather parameters have stabilized. During the main phase, the strong negative Bz and high solar wind speed would have led to increased ionospheric currents and possibly enhanced ionospheric scintillation, especially over the West African region. The effects would include changes in the electron density and possible disruptions in communication and navigation systems in the area. This analysis indicates that the November 5-6, 2023, geomagnetic storm was a significant event with marked changes in solar wind conditions, interplanetary magnetic field orientation, and geomagnetic indices, all of which would have impacted the ionosphere over the West African sector.

The geomagnetic storm have lingering effects even after the recovery phase begins i.e November 6, 2023 as revealed in the result. This lingering effects result from slower processes such as recombination, thermospheric circulation, and residual ring current dissipation. These processes take longer to

stabilize, maintaining minor disturbances in TEC and magnetic field variations even after the main storm effects have subsided.

3.2. TEC Variation During the November 5-6, 2023 Storm

Studying the ionospheric response during geomagnetic storms is crucial for understanding the complex interactions between the solar wind, magnetosphere, and ionosphere. Analyzing various parameters such as Bz, SYM-H, solar wind speed, and pressure can provide insights into the severity and characteristics of ionospheric storms. Following the sudden storm start (SSC), geomagnetic storms typically go through three phases: the primary phase, the early phase, and the recovery phase [10]. Black line shows TEC on November 5, 2023, Cyan line represents TEC on November 6, 2023, and the blue dashed line shows Mean TEC on quiet days as shown in Figure 3.

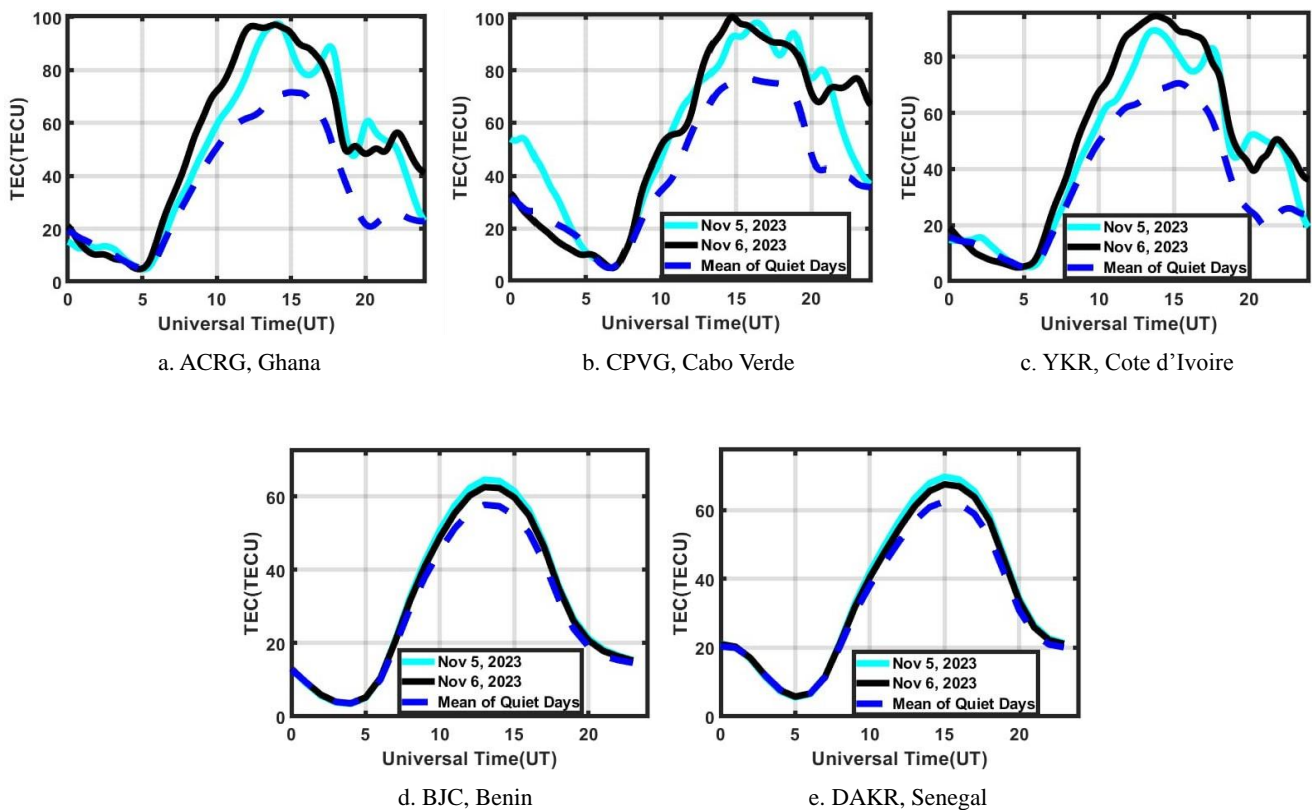


Figure 3. Variations of TEC against universal time during the storm.

For the station ACRG, Ghana Figure 3a, on November 5, 2023 (Black Line), morning Hours (0-6 UT), the TEC starts off low, similar to the mean value for quiet days, indicating that the ionosphere was relatively undisturbed early in the day. At 6-12 UT, there is a rapid increase in TEC is observed, reaching a peak around 80 TECU. This is significantly higher

than the quiet day average, indicating strong ionospheric disturbances likely driven by the geomagnetic storm. But at 12-18 UT, the TEC begins to decrease but remains elevated compared to the quiet day mean, showing that the ionosphere was still heavily influenced by storm conditions. Similarly, at 18- 24 UT, the TEC continues to decline, moving closer to the

quiet day values, but still showing signs of disturbance. On November 6, 2023 (Cyan Line) during morning Hours (0-6 UT), the TEC starts low and follows a similar pattern to the previous day, showing slight disturbances, and at 6-12 UT it rises sharply again, though not as high as on November 5, reaching a peak of around 70 TECU. But at 12-18 UT, there is a more significant drop in TEC occurs, falling below the peak values but still higher than the quiet day mean and at 18-24 UT it continues to drop, showing a more rapid return to normal quiet day conditions, although some minor fluctuations persist. Both storm days show a significant increase in TEC during the daytime hours (6-18 UT), which is a typical response to enhanced ionospheric activity driven by geomagnetic storms.

In comparison to Quiet Days, the TEC during the storm days is substantially higher than the quiet day average, highlighting the storm's impact on the ionosphere. In recovery Phase, the ionosphere begins to recover on November 6, with TEC values decreasing and approaching the quiet day levels, but still exhibiting storm-induced fluctuations.

From Figure 3b, the TEC Values on Quiet Days (Blue Dashed Line) typically peaks around 50 TECU (Total Electron Content Units) at approximately 14:00 UT and then gradually decreases, and TEC on November 5, 2023 (Light Blue Line), the TEC follows the trend similar to quiet days but shows a slightly higher peak around the same time, reaching approximately 55 TECU. This indicates an enhancement in TEC, which is characteristic of a positive ionospheric storm, while on November 6, 2023 (Black Line), the TEC curve is almost aligned with the quiet day trend, with a minor difference, suggesting a relatively mild or returning-to-normal ionospheric condition. Overall, the geomagnetic storm on November 5, 2023, led to a positive ionospheric storm over Cabo Verde, causing a temporary increase in the TEC values. The storm's impact diminished by November 6, 2023, with TEC values aligning more closely with quiet day levels.

For YKR station in Cote d'Ivoire Figure 3c, during the Mean of Quiet Days typically, the TEC increases gradually, peaks around the early afternoon (local time), and then decreases, and On November 5, the TEC follows a similar trend to the quiet day average initially. Around 10:00 UT, it begins to rise sharply, reaching a higher peak than the mean of quiet days. The TEC remains elevated until approximately 18:00 UT, after which it decreases and eventually dips below the quiet day level in the late evening. But, on November 6, the TEC is initially lower than on November 5 and remains above the quiet day mean. After 10:00 UT, it shows a sharp increase, similar to November 5, reaching a slightly higher peak. The TEC drops sharply after 17:00 UT, falling below the quiet day average towards the end of the day. Similarly the geomagnetic storm from November 5-6, 2023, in Cote d'Ivoire primarily exhibited a positive storm phase, with TEC values significantly exceeding those of quiet days, especially during the peak hours of the day. There are also signs of a negative phase later in the day, indicating a complex storm structure.

According to Figure 3d, the geomagnetic storm from November 5-6, 2023, in Benin primarily exhibited characteristics of a weak positive storm, with TEC values slightly exceeding those of quiet days, especially during the afternoon hours. The variation is subtle, indicating that the storm's impact was not very strong in this region. On November 5, the TEC closely follows the quiet day average until about 10:00 UT. After this time, the TEC begins to rise, slightly exceeding the quiet day mean. The peak TEC on this day is slightly higher than the mean of quiet days, but it stays close to the expected quiet day behavior, and on November 6, the TEC also follows the quiet day average closely in the early hours. After 10:00 UT, the TEC again rises, peaking slightly higher than the quiet day mean, similar to November 5. After peaking, the TEC decreases and aligns closely with the quiet day mean towards the evening. Similar to Benin, Senegal experienced a weak positive storm. The TEC was marginally higher than the quiet day mean during peak hours, with no significant negative phase as shown in Figure 3e. It primarily exhibited characteristics of a weak positive storm, with TEC values slightly exceeding those of quiet days, especially during the afternoon hours. The storm's impact was modest, with TEC variations closely following the expected quiet day behavior.

3.3. O/N₂ Distribution over the West African Sector During November 5-6, 2023

We used globally [O]/[N₂] maps, which provide the global thermospheric neutral composition variations obtained from Global Ultraviolet Imager (GUVI) instrument onboard TIMED (Thermosphere Ionosphere Mesosphere Energetics and Dynamics) space craft. The [O]/[N₂] ratio is an important indicator of the thermospheric neutral composition, where higher values (indicated in red) correspond to regions with a greater proportion of atomic oxygen relative to molecular nitrogen, and lower values (indicated in blue) indicate a higher proportion of molecular nitrogen. Time points on the top plots denote points of the satellite orbits around the equator.

The overall pattern of the O/N₂ ratio remains consistent across both dates, with higher ratios near the equator and lower ratios near the poles. Both images display a similar color gradient, with red indicating higher ratios and blue indicating lower ratios. The color bands near the equator and mid-latitudes are fairly consistent, showing little variation in the general distribution of the [O]/[N₂] ratio. On November 5, the [O]/[N₂] ratio appears slightly more intense (red/yellow) around the equatorial region compared to November 6, while on November 6, there seems to be a slight decrease in the O/N₂ ratio intensity in some areas, particularly around Africa and the Indian Ocean, indicating a possible relaxation in the geomagnetic storm's effects.

The comparison illustrated by Figure 4 suggests that the geomagnetic storm's influence was slightly stronger on November 5, 2023, with a gradual decrease in its effects by

November 6. During geomagnetic storms, energy input from the solar wind heats and disturbs the thermosphere, causing changes in the O/N_2 ratio. Regions with enhanced O/N_2 ratios often align with geomagnetic equators or areas of strong upward thermospheric winds, and low O/N_2 ratios are more common in higher latitudes or during the storm recovery phase, correlating with downwelling of nitrogen-rich air as revealed by the result obtained.

The thermospheric neutral composition ratio $[O]/[N_2]$ during the quiet periods of November 3, 4, 7, and 8, 2023, reveals a stable and typical distribution of atomic oxygen (O) relative to molecular nitrogen (N_2) in the West African sector.

In these maps, the O/N_2 ratio is higher at higher latitudes, particularly in the northern hemisphere, where yellow-to-red regions indicate a dominance of atomic oxygen. In contrast, the equatorial region, including West Africa (latitude $\sim 0-20^\circ$ N, longitude $\sim 10^\circ$ W- 10° E), predominantly exhibits lower O/N_2 ratios, represented by green to blue hues, signifying a relatively higher abundance of molecular nitrogen. This pattern aligns with the thermospheric dynamics at equatorial latitudes, where neutral composition is influenced by upward and downward motions driven by solar heating and equatorial ionospheric processes such as the fountain effect.

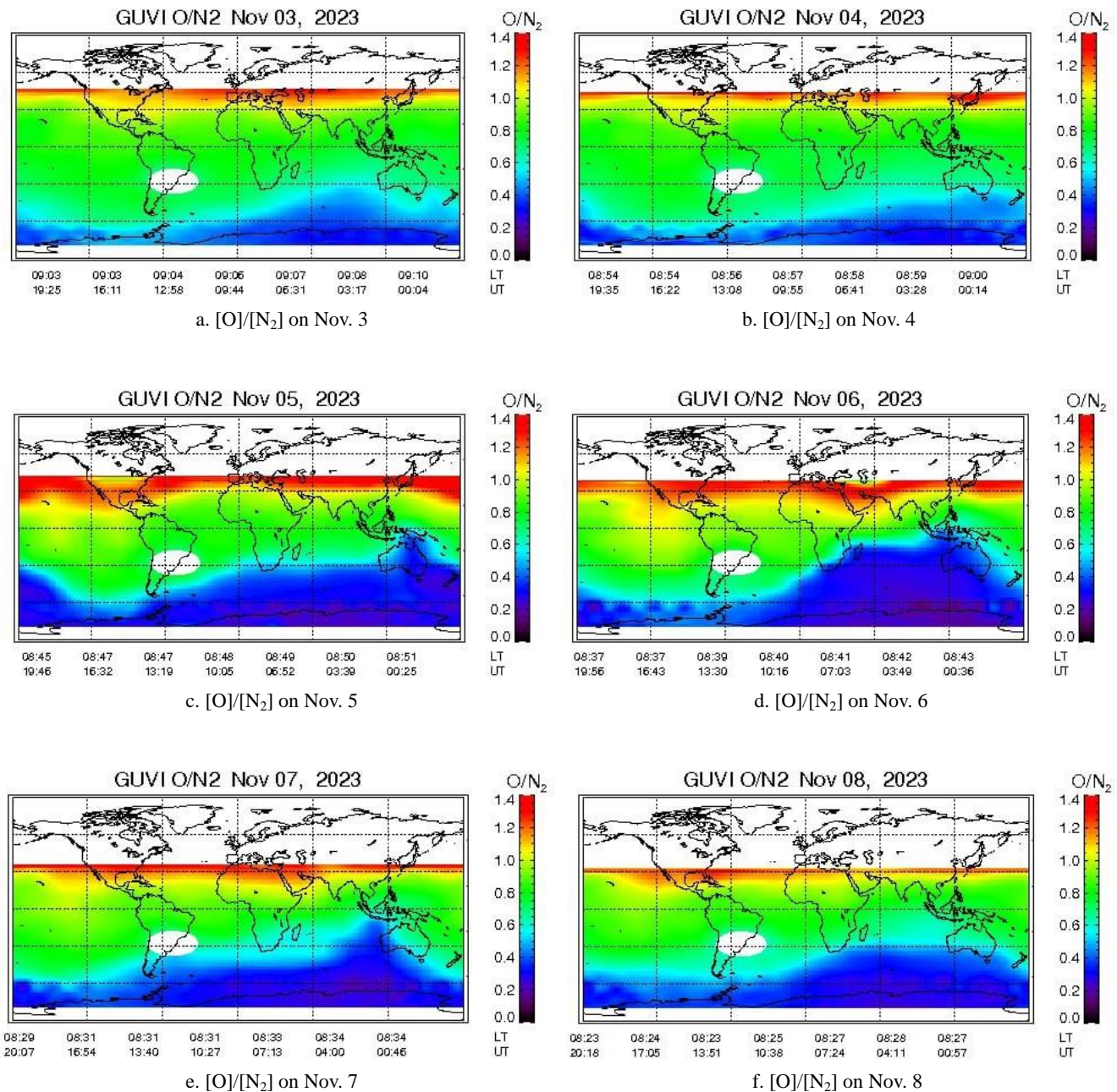


Figure 4. O/N_2 distribution over the West African sector during November 5-6, 2023.

The consistency of the O/N₂ ratio over these quiet days reflects minimal external forcing from geomagnetic or solar activity, providing a baseline state of the thermosphere. During geomagnetic quiet conditions, the thermosphere and ionosphere remain in a steady equilibrium, with no significant disturbances in the neutral composition. This baseline is crucial for identifying and interpreting storm-induced changes during the geomagnetic storm of November 5-6, 2023. Typically, during geomagnetic storms, energy input from high latitudes causes thermospheric upwelling, reducing the O/N₂ ratio at lower altitudes and affecting equatorial regions. These quiet-time observations thus serve as a reference for assessing how the storm perturbed the neutral composition and its subsequent impact on ionospheric behavior over the West African sector.

3.4. Analysis of PPEF During the Storm

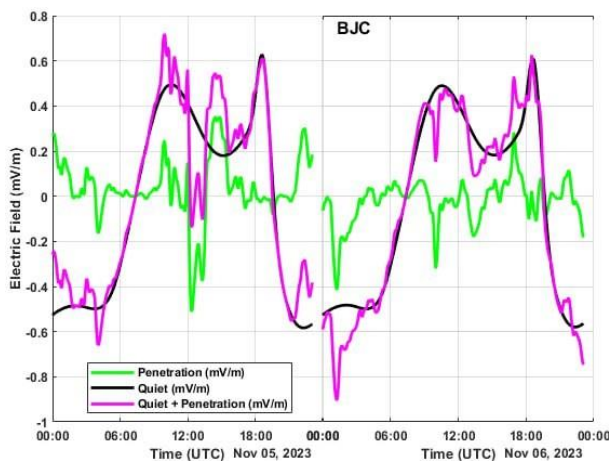
The following Figure 5 shows the Penetration Electric Field (PEF), Quiet Electric Field (QEF), and the combined effect (QEF + PEF) over the six days during quiet time and the storm period. In November 5, 2023; there is significant variation in the electric field magnitude throughout the day. The penetration electric field (green) shows multiple peaks and troughs, indicating strong storm-time effects. The quiet-time electric field (black) shows smaller variations compared to the penetration field. The combined effect (black) follows the penetration electric field closely, suggesting that the storm-time electric fields dominate over the quiet-time fields during the main phase as shown for BJC station, Benin in Figure 5.

a. Similar patterns of electric field variations are observed in November 6, though the intensity of the penetration electric field seems slightly reduced compared to November 5. The quiet-time electric field remains consistent and smooth, while the penetration electric field displays fluctuations due to storm-time dynamics. The combined effect (black) once again demonstrates that the storm-time Penetration fields significantly influence the total electric field.

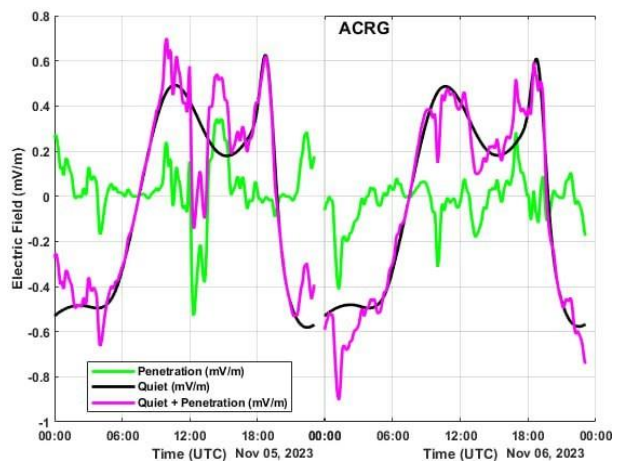
Figure 5b, Similar trends to BJC, with noticeable peaks

around 12:00 UTC and 18:00 UTC on November 5. Oscillations between negative and positive values reflect the rapid variability of PPEFs during the storm. The quiet field shows a consistent, low-magnitude trend across the 48-hour period. The magenta curve shows enhancements during the storm periods, correlating strongly with the peaks in the penetration field. In Figure 5c, it was shown that the penetration electric field exhibits sharp peaks and troughs, showing significant variability in November 5. This indicates strong penetration of storm-time electric fields into the YKR station, Cote d'Ivoire. The quiet-time electric field (purple) remains relatively smooth compared to the storm-induced penetration fields. The combined electric field closely follows the shape of the penetration field, highlighting its dominance during the storm. Around local midday and evening hours (12:00-18:00 UTC), the electric field peaks are most prominent, suggesting intensified storm-time electric fields during these periods.

Similar patterns of variability in the penetration electric field are observed in November 6, though the intensity appears slightly reduced compared to November 5. The combined electric field continues to align with the penetration field, with noticeable fluctuations at midday and evening hours. Again, from Figure 5d CPVG station Capo Verde in November 5, 2023; Penetration Field (Green) Peaks are observed around 12:00 UTC and 18:00 UTC on November 5, indicating significant penetration electric fields during the geomagnetic storm's main phase. The field transitions between positive and negative values, showing variability in penetration efficiency. This reflects the direct response of the ionosphere to interplanetary electric fields (IEFs). The quiet-time electric field (Black) remains relatively steady and small in magnitude compared to the penetration field, reflecting regular ionospheric dynamics unaffected by geomagnetic disturbances. The combined electric field amplifies during the storm periods, showing peaks aligning with the penetration field. This highlights the impact of PPEFs on the ionosphere. From figure 5e DAKR station, Senegal, clear peaks of Penetration field occur at approximately 12:00 UTC and 18:00 UTC on November 5, with values exceeding those during quiet times.



a. PPEFs in BJC, Benin



b. PPEFs in ACRG, Ghana

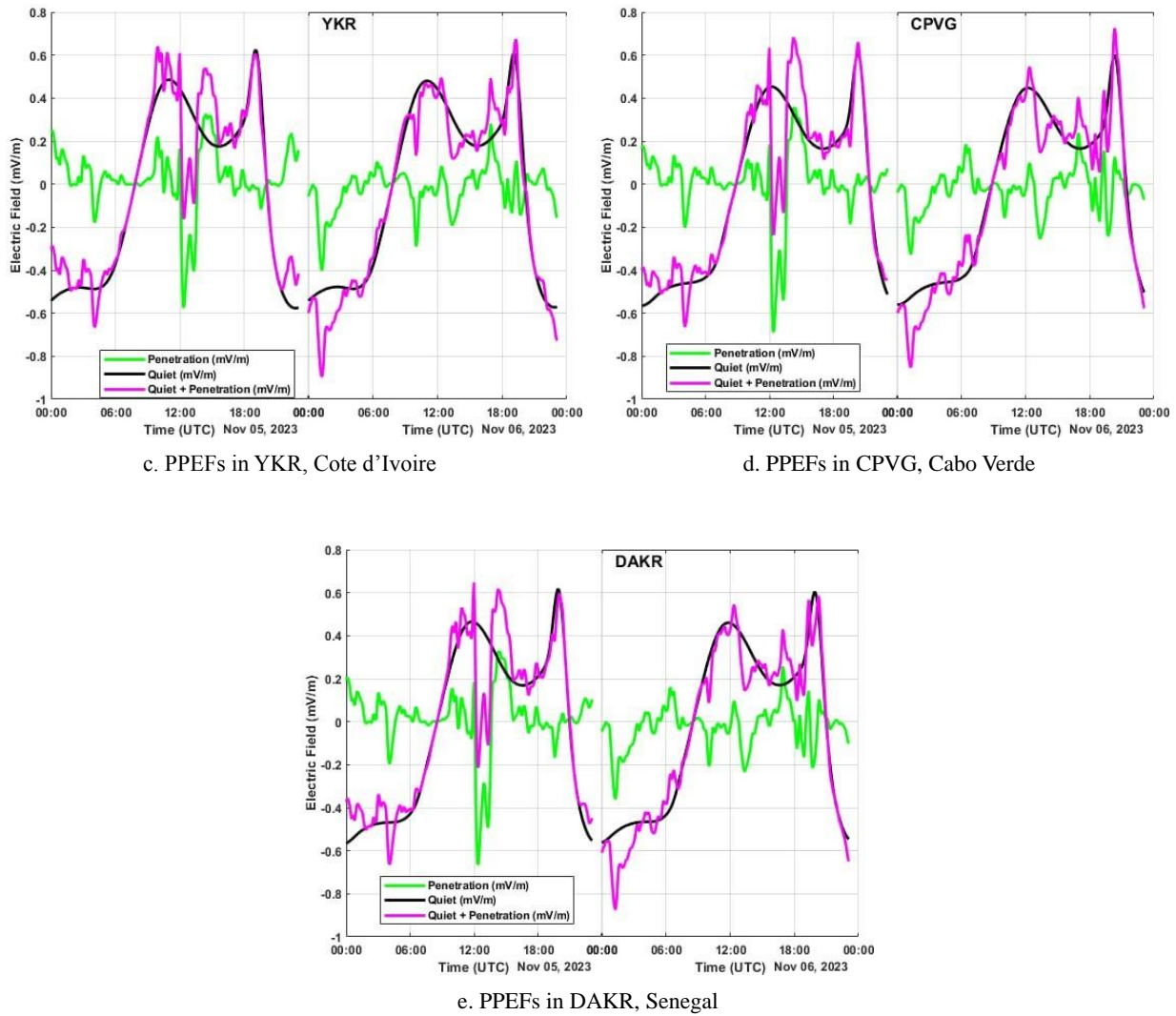


Figure 5. Effects of PPEFs over the west Africa during the main phase of the storms.

Negative and positive oscillations are present, indicating prompt penetration effects are occurring due to external solar wind and magnetospheric interactions. Stable baseline is evident throughout the day, confirming the quiet-time dynamics at this location. For Quiet + Penetration Field, significant enhancement of the field is observed, particularly during the peaks of the penetration field. This indicates that the geomagnetic storm's main phase strongly influenced the electric field. On November 6, penetration fields remain active during local nighttime hours, suggesting that undershielding electric fields persisted. This extended PPEF effect could sustain ionospheric disturbances into the recovery phase of the storm.

The strong perturbations observed in the combined electric field (QEF + PEF) during both days indicate that the ionosphere in the West African sector was significantly impacted by the geomagnetic storm. The increase in the electric field strength during daytime hours may result in increased ionospheric conductivity and disturbances in the E and F region, potentially leading to ionospheric irregularities like scintillations or disruptions in GPS signals. Negative deviations in the

combined signal during the night (after 18:00 UTC). These indicate the presence of westward electric fields, which are characteristic of the Disturbance Dynamo Effect. Such behavior can lead to the suppression of the ionospheric plasma density, affecting the equatorial ionization anomaly and potentially causing disruptions in communication and navigation signals.

The strong perturbations observed in the combined electric field (QEF + PEF) during both days indicate that the ionosphere in the West African sector was significantly impacted by the geomagnetic storm. The increase in the electric field strength during daytime hours may result in increased ionospheric conductivity and disturbances in the E and F region, potentially leading to ionospheric irregularities like scintillations or disruptions in GPS signals. Negative deviations in the combined signal during the night (after 18:00 UTC). These indicate the presence of westward electric fields, which are characteristic of the Disturbance Dynamo Effect. Such behavior can lead to the suppression of the ionospheric plasma density, affecting the equatorial ionization anomaly and potentially causing disruptions in communication and navigation

tion signals.

4. Discussion

The November 5-6, 2023 geomagnetic storm presented a unique opportunity to study the ionospheric response over the West African sector, a region that is particularly vulnerable to geomagnetic disturbances due to its proximity to the geomagnetic equator. Basically, depending on tranquil or pre-storm conditions, the ionospheric electron density can either rise or fall. Usually, these are referred to as positive and negative storm effects or positive and negative ionospheric storms, respectively [17]. The storm was characterized by a sudden increase in solar wind speed, a significant southward turning of the Bz component of the interplanetary magnetic field, and a sharp drop in the Sym-H index, triggered substantial ionospheric disturbances across the region.

The variations in TEC observed during the geomagnetic storm were particularly notable across the different GNSS stations in West Africa. Our analysis of Total Electron Content (TEC) revealed marked variations during the storm, with significant positive ionospheric storm phases observed in countries such as Ghana and Cote d'Ivoire, with TEC values on both November 5 and 6 are significantly higher than the quiet day mean, especially during the early afternoon hours (10:00 UT to 18:00 UT). This indicates that the storm caused an increase in ionization levels in the ionosphere, characteristic of a positive storm. However, there are moments, especially late in the day on November 5 and 6, where the TEC drops below the quiet day average, which is a characteristic of a negative storm. During the GMS recovery phase, the DDEF acts westward/eastward during the day and night, propelled by storm time neutral wind [29].

According to Fejer et al., (2007), during the day, the disturbance dynamo electric field (DDEF) reduces ionospheric drift, improving recombination rate and, as a result, decreasing TEC and producing a negative ionospheric storm effect [30]. During the night, however, the DDEF increases ionospheric $E \times B$ upward drift, transporting plasma to elevated altitudes and, as a result, minimizing recombination rate and producing a positive ionospheric storm effect. However, the primary behavior observed during peak hours points to a positive storm. Benin and Senegal had similar, weaker storm impacts, characterized by modest positive TEC variations. No region experienced a strong negative storm phase, with Cote d'Ivoire and Ghana showing the most dynamic response to the geomagnetic activity. These regions experienced a sharp increase in TEC during the daytime hours, reflecting enhanced ionization likely driven by the intense coupling of solar wind energy into the Earth's magnetosphere. The TEC levels in these areas remained elevated well into the recovery phase, indicating a prolonged impact of the storm.

In contrast, the TEC variations in Senegal, Cabo Verde and Benin were less pronounced, suggesting a weaker storm influence in these regions. It is well known that changes in the

thermospheric composition caused by the heating of the thermosphere during geomagnetic storms are usually used to explain the negative storm effects (decreases in the peak electron density [31]. The relative proximity of these stations to the geomagnetic equator might account for the observed differences, as the equatorial ionosphere is known to respond differently to geomagnetic disturbances compared to higher latitudes. The analysis of the O/N₂ ratio further supports these findings, showing a slight relaxation of storm effects by November 6. The reduced intensity of the O/N₂ ratio in some areas, particularly around Africa, suggests that the thermospheric response was beginning to return to normal, although lingering disturbances were still present. The large-scale thermospheric circulation transports air rich in atomic oxygen toward lower latitudes. This increased oxygen density alters both ionization production and diffusion, leading to positive storm effects [31-34].

Moreover, thermospheric composition changes such as O/N₂ density depletion play a significant role in negative ionospheric storm effects over low to mid-latitude region [35, 36]. Diverse reports exist on variations in the ionosphere during storm phases at various longitudes. For instance, according to Lissa et al., (2020), the ionosphere might react to storms in a similar way at times or very differently at mid-latitude, depending on 30 degrees longitude [37]. Significant variations were observed in the ionosphere at 80 degree E and 120 degree E longitudes by Liu et al., (2019) which may have resulted from eastward Prompt Penetration Electric Field (PPEF) associated with a strongly enriched O/N₂ ratio of thermosphere neutral composition [38]. The initial assessment of the PPEFM's performance over the African longitude showed that the model successfully replicates the enhancement and suppression of the PRE driven by eastward and westward PPEF, along with the associated impact on the behavior of irregularities during storm events [28]. The penetration electric field (green line) displayed strong fluctuations with pronounced peaks and troughs, indicating intense storm-time effects.

The combined electric field closely mirrored the penetration electric field, highlighting its dominance during the geomagnetic disturbance. The largest variations occurred during midday and evening hours (12:00-18:00 UTC), corresponding to periods of maximum ionospheric disturbance. The penetration electric field variability was reduced compared to November 5, indicating a gradual weakening of the storm's intensity. Similar to November 5, the combined electric field was dominated by the penetration component, with notable peaks around midday and evening hours. The penetration electric field (PEF) during the geomagnetic storm on November 5-6, 2023, caused significant perturbations in the ionospheric electric field over the West African sector, leading to strong deviations from normal quiet-time conditions. These perturbations are indicative of increased ionospheric dynamics, which can adversely impact radio wave propagation and satellite-based communication. Nayak et al., (2016) had used

the PPEFM to highlight the effect of eastward PPEF/westward DDEF on the PRE during the storm, that is consistent to our result [39].

5. Conclusion

The study of geomagnetic storm is an important issue for the study of space weather. The Bz component is an important parameter which indicates the presence of geomagnetic storm. In this research, we study several solar wind parameters and geomagnetic indices. The November 5-6, 2023 geomagnetic storm presented a unique opportunity to study the ionospheric response over the West African sector, a region that is particularly vulnerable to geomagnetic disturbances due to its proximity to the geomagnetic equator. The storm, characterized by a sudden increase in solar wind speed, a significant southward turning of the Bz component of the interplanetary magnetic field, and a sharp drop in the Sym-H index, triggered substantial ionospheric disturbances across the region. Our analysis of Total Electron Content (TEC) revealed marked variations during the storm, with significant positive ionospheric storm phases observed in countries such as Ghana and Cote d'Ivoire. These regions experienced a sharp increase in TEC during the daytime hours, reflecting enhanced ionization likely driven by the intense coupling of solar wind energy into the Earth's magnetosphere.

The TEC levels in these areas remained elevated well into the recovery phase, indicating a prolonged impact of the storm. In contrast, regions like Senegal and Benin exhibited weaker responses, with TEC values only slightly exceeding those of quiet days. This variability in storm impact across the West African sector underscores the complex nature of ionospheric responses to geomagnetic storms, which can be influenced by a range of factors including geographic location, local time, and pre-existing ionospheric conditions. The storm also had a noticeable effect on the thermospheric composition, as indicated by changes in the O/N₂ ratio. The data suggests that the thermosphere experienced a slight relaxation in storm effects by November 6, but with some residual disturbances. Additionally, the enhancements and fluctuations of Penetration Electric Field are indicative of increased ionospheric disturbances, which have implications for space weather phenomena and can adversely affect ground-based and satellite communication systems in the region.

The penetration fields alternate between positive and negative values, reflecting the dynamic behavior of PPEFs during storm-time. This oscillation is indicative of rapid magnetospheric-ionospheric coupling and potential polarity changes in the external driving electric fields. November 5 experienced stronger electric field fluctuations compared to November 6, indicating that the ionospheric response was more pronounced on the first day of the storm. Therefore, the PPEFM effectively captured the behavior of the PPEF, which intensified or suppressed the PRE during the postsunset period in the main phase of the March 5-6, 2023, storms. The

storm induced enhanced eastward electric fields, which likely strengthened the Equatorial Electrojet (EEJ) and caused ionospheric instabilities. These instabilities could have led to the development of equatorial plasma bubbles, disrupting radio wave propagation and satellite-based navigation systems. The strongest ionospheric responses were observed during midday and evening hours, highlighting the diurnal modulation of PPEF impacts. November 5 experienced stronger electric field fluctuations compared to November 6, indicating that the ionospheric response was more pronounced on the first day of the storm.

6. Recommendation

This study provides valuable insights into ionospheric dynamics during geomagnetic storms, particularly in low-latitude regions such as West Africa. To build upon these findings, future research should expand the analysis to include additional ionospheric parameters, such as F-region electron density and ionospheric drifts, for a more comprehensive understanding of storm-time variations. Additionally, developing localized space weather models and forecasting tools tailored to West Africa would enhance preparedness for geomagnetic storm-induced disruptions in communication and navigation systems. Further investigations into the role of thermospheric composition, particularly the O/N₂ ratio, are also needed to better understand its influence on ionospheric variability during geomagnetic disturbances. Finally, enhancing ground-based GNSS observation networks across West Africa would improve spatial coverage and data accuracy, enabling more precise monitoring of ionospheric anomalies.

Abbreviations

TEC	Total Electron Content
EEJ	Equatorial Electrojet
PPEFM	Prompt Penetration Electric Field Model
IMF	Interplanetary Magnetic Field
V _{sw}	Solar Wind Speed
GNSS	Global Navigation Satellite System
GPS	Global Positioning System
Dst	Disturbance Storm Time
SYM-H	Symmetric-Horizontal Index
GUVI	Global Ultraviolet Imager
TIMED	Thermosphere Ionosphere Mesosphere Energetics and Dynamics
CME	Coronal Mass Ejection
EEF	Equatorial Electric Field
NOAA	National Oceanic and Atmospheric Administration
NASA	National Aeronautics and Space Administration
IEFs	Interplanetary Electric Fields
DDEF	Disturbance Dynamo Electric Field

Acknowledgments

We express our deepest gratitude to the World Data Center at Kyoto University, Japan, for supplying the Sym-H data (available at <http://wdc.kugi.kyoto-u.ac.jp/dstae/index.html>), to the OMNI database (<https://omniweb.gsfc.nasa.gov>) for providing interplanetary and solar wind parameters, and to the AFREF (<http://www.afrefdata.org/>) and IGS (<http://igs.org>) for providing TEC data, special thanks to the NOAA Space Weather Prediction Center (SWPC) for providing prompt penetration electric field data that was extracted from (<https://geomag.colorado.edu/online-calculators/real-time-model-ionospheric-electric-fields>). Additionally, to the GUVI-TIMED data providers NASA's MO & DA program that was obtained from http://guvitimed.jhuapl.edu/data_status_l3_on2_idlsave.

Author Contributions

Gebre Kalute: Conceptualization, Data curation, Formal Analysis, Funding acquisition, Investigation, Methodology, Resources, Software, Visualization, Writing -original draft, Writing-review

Dejene Ambisa: Project administration, Supervision, Validation

Selemon Sisay: Software, Writing-original draft

Tegegn Teferi: Formal Analysis, Resources, Validation, Writing-review & editing

Conflicts of Interest

The authors declare no conflicts of interest.

References

- [1] Golubkov, G. V., M. I. Manzhelii, and I. V. Karpov. "Chemical physics of the upper atmosphere." *Russian Journal of Physical Chemistry B* 5 (2011): 406-411.
- [2] Buonsanto, M. Ji. "Ionospheric storms-A review." *Space Science Reviews* 88.3 (1999): 563-601.
- [3] Sorokin, Valery M., Vitaly M. Chmyrev, and Masashi Hayakawa. "A review on electrodynamic influence of atmospheric processes to the ionosphere." *Open Journal of Earthquake Research* 9.2 (2020): 113-141.
- [4] Achilleos, Nicholas, Licia Ray, and Japheth Yates. "Magnetosphere-Ionosphere Coupling." Oxford University Press, 2021.
- [5] Tsagouri, Ioanna, et al. "Ionosphere variability I: Advances in observational, monitoring and detection capabilities." *Advances in Space Research* (2023).
- [6] Kintner Jr, Paul M., et al., eds. *Midlatitude ionospheric dynamics and disturbances*. Vol. 181. John Wiley & Sons, 2013.
- [7] Tasic, Mirjana, et al. "Atmospheric aerosols and their influence on air quality in urban areas." *Facta universitatis-series: Physics, Chemistry and Technology* 4.1 (2006): 83-91.
- [8] Koshovyy, V., et al. "Influence of active cosmic factors on the dynamics of natural infrasound in the Earth's atmosphere." *Romanian Journal of Physics* 65 (2020): 813.
- [9] Alex, S., S. Mukherjee, and G. S. Lakhina. "Geomagnetic signatures during the intense geomagnetic storms of 29 October and 20 November 2003." *Journal of atmospheric and solar-terrestrial physics* 68.7 (2006): 769-780.
- [10] Gonzalez, W. D., et al. "What is a geomagnetic storm." *Journal of Geophysical Research: Space Physics* 99. A4 (1994): 5771-5792.
- [11] Kumar, Sushil, and Vickal V. Kumar. "Ionospheric response to the St. Patrick's Day space weather events in March 2012, 2013, and 2015 at southern low and middle latitudes." *Journal of Geophysical Research: Space Physics* 124.1 (2019): 584-602.
- [12] Davis, C. J., et al. "Ionospheric and geomagnetic responses to changes in IMF B z: a superposed epoch study." *Annales Geophysicae*. Vol. 15. Springer-Verlag, 1997.
- [13] Ariyibi, Emmanuel A., Emanuel O. Joshua, and Babatunde A. Rabi. "Studies of ionospheric variations during geomagnetic activities at the low-latitude station, Ile-Ife, Nigeria." *Acta Geophysica* 61 (2013): 223-239.
- [14] Baker, D. N., Niescja E. Turner, and T. I. Pulkkinen. "Energy transport and dissipation in the magnetosphere during geomagnetic storms." *Journal of Atmospheric and Solar-Terrestrial Physics* 63.5 (2001): 421-429.
- [15] Schmieder, Brigitte. "Extreme solar storms based on solar magnetic field." *Journal of Atmospheric and Solar-Terrestrial Physics* 180 (2018): 46-51.
- [16] Wood, Brian E., et al. "Comparative ionospheric impacts and solar origins of nine strong geomagnetic storms in 2010-2015." *Journal of Geophysical Research: Space Physics* 121.6 (2016): 4938-4965.
- [17] Mansilla, Gustavo A., and Marta M. Zossi. "Ionospheric response to the 26 August 2018 geomagnetic storm along 280 E and 316 E in the South American sector." *Advances in Space Research* 69.1 (2022): 48-58.
- [18] Davies, K. "Ionospheric Radio, IEE Electromagn." *Waves Ser* 31 (1990): 476-483.
- [19] Sobral, J. H. A., et al. "Effects of intense storms and substorms on the equatorial ionosphere/thermosphere system in the American sector from ground-based and satellite data." *Journal of Geophysical Research: Space Physics* 102. A7 (1997): 14305-14313.
- [20] Olawepo, A. O. "Response of ionospheric N (h) profiles over Ilorin to moderate geomagnetic storms, Ife J." *Sci* 15.3 (2013): 509-521.
- [21] Olawepo, A. O., and J. O. Adeniyi. "Ionosphere's F2-layer response to 2006 geomagnetic storm at Ilorin, Nigeria." *The African Review of Physics* 7 (2012).

- [22] Omojola, Joseph, and Taiwo Adewumi. "Effects of St Patrick's day intervals geomagnetic storms on the accuracy of GNSS positioning and total electron content over nigeria." *J Earth Space Phys* 45.4 (2020): 181-188.
- [23] Astafyeva, Elvira, Irina Zakharenkova, and Matthias Forster. "Ionospheric response to the 2015 St. Patrick's Day storm: A global multi-instrumental overview." *Journal of Geophysical Research: Space Physics* 120.10 (2015): 9023-9037.
- [24] Zolotukhina, N., et al. "Ionospheric effects of St. Patrick's storm over Asian Russia: 17-19 March 2015." *Journal of Geophysical Research: Space Physics* 122.2 (2017): 2484-2504.
- [25] Pathy, Nyanasegari Bhoo, et al. "Near real time ionospheric monitoring system over Malaysia using GPS Data: My-Iono Service." *Journal of Physics: Conference Series*. Vol. 1152. No. 1. IOP Publishing, 2019.
- [26] Seemala, G. K., and C. E. Valladares. "Statistics of total electron content depletions observed over the South American continent for the year 2008." *Radio Science* 46.05 (2011): 1-14.
- [27] Christensen, A. B., et al. "Initial observations with the Global Ultraviolet Imager (GUVI) in the NASA TIMED satellite mission." *Journal of Geophysical Research: Space Physics* 108. A12 (2003).
- [28] Amaechi, Paul O., et al. "Geomagnetic activity control of irregularities occurrences over the crests of the African EIA." *Earth and Space Science* 7.7 (2020): e2020EA001183.
- [29] Blanc, M., and A. D. Richmond. "The ionospheric disturbance dynamo." *Journal of Geophysical Research: Space Physics* 85. A4 (1980): 1669-1686.
- [30] Fejer, Bela G., John W. Jensen, and Shin Yi Su. "Quiet time equatorial F region vertical plasma drift model derived from ROCSAT-1 observations." *Journal of Geophysical Research: Space Physics* 113. A5 (2008).
- [31] Fuller-Rowell, T. J., et al. "Response of the thermosphere and ionosphere to geomagnetic storms." *Journal of Geophysical Research: Space Physics* 99. A3 (1994): 3893-3914.
- [32] Danilov, A. D., et al. "Positive phase of ionospheric storms and its connection with the dayside cusp." *Advances in space research* 7.8 (1987): 81-88.
- [33] Rishbeth, H., T. J. Fuller-Rowell, and Alan S. Rodger. "F-layer storms and thermospheric composition." *Physica Scripta* 36.2 (1987): 327.
- [34] Prolss, Gerd W. "Ionospheric F-region storms." *Handbook of Atmospheric Electrodynamics* (1995). CRC press, 2017. 195-248.
- [35] Strickland, D. J., R. E. Daniell, and J. D. Craven. "Negative ionospheric storm coincident with DE 1-observed thermospheric disturbance on October 14, 1981." *Journal of Geophysical Research: Space Physics* 106. A10 (2001): 21049-21062.
- [36] Liou, K., et al. "Neutral composition effects on ionospheric storms at middle and low latitudes." *Journal of Geophysical Research: Space Physics* 110. A5 (2005).
- [37] Lissa, D., et al. "Ionospheric response to the 26 August 2018 geomagnetic storm using GPS-TEC observations along 80 E and 120 E longitudes in the Asian sector." *Advances in Space Research* 66.6 (2020): 1427-1440.
- [38] Liu, Libo, et al. "New aspects of the ionospheric behavior over Millstone Hill during the 30-day incoherent scatter radar experiment in October 2002." *Journal of Geophysical Research: Space Physics* 124.7 (2019): 6288-6295.
- [39] Nayak, Chinmaya, et al. "Suppression of ionospheric scintillation during St. Patrick's Day geomagnetic super storm as observed over the anomaly crest region station Pingtung, Taiwan: A case study." *Advances in Space Research* 60.2 (2017): 396-405.